Proceedings of ASME Turbo Expo 2011
GT2011
June 6-10, 2011, Vancouver, British Columbia, Canada

GT2011-46366

EXPERIMENTAL INVESTIGATION OF THE INFLUENCE OF WATER INJECTION ON ACOUSTIC PROPERTIES OF THE EXHAUST SYSTEM OF A GAS TURBINE COMBUSTION TEST RIG

Martin Schmid*, Natalie Trott, Robert Kathan, Dan Fanaca
Thomas Sattelmayer
Lehrstuhl für Thermodynamik
Technische Universität München
85748 Garching
Germany

ABSTRACT

It is a known phenomenon that single can combustion test rigs and gas turbines have a different stability behavior. Real gas turbines are often more stable than their test rigs. One main difference between test rigs and real engines is the injection of cooling water into the test rigs to reduce the temperature of the exhaust gas and thus to protect the exhaust valve.

A literature survey showed that the presence of a two phase flow can drastically reduce the sonic velocity and consequently change the acoustic properties of a system. The aim of this project is to study the influence of water injection on the acoustic properties of a test rig representing the exhaust system of a gas turbine.

The experimental results clearly show that the sonic velocity does not change in the present test rig because the droplets are too big to follow the acoustic fluctuations. The critical dimensionless number in this context is the Stokes number, which is mainly determined by the droplet diameter and the acoustic frequency. Furthermore, the experimental results point out that the injected water increases the acoustic damping.

It can be concluded from this study that the influence of water injection on the acoustic properties and therefore on the stability behavior is very sensitive to the injection conditions, especially the droplet diameter.

NOMENCLATURE

A	Area
α	Void fraction
AMF	Air Mass Flow
c	Sonic velocity
d_p	Droplet diameter
η	Gas viscosity
f	Frequency
f	Downstream traveling Riemann invariant
g	Upstream traveling Riemann invariant
$\langle I \rangle$	Time-averaged acoustic flux per area
$\langle K \rangle$	Dimensionless time-averaged acoustic flux per area
$k_x^{\pm}$	Wave number
L	Length
M	Mach number
μ	Mass fraction
ω	Angular frequency
$\hat{p}$	Complex pressure amplitude
r	Reflection coefficient
$\bar{\rho}$	Mean density
$\hat{u}$	Complex velocity amplitude
$\bar{u}$	Mean flow velocity
WMF	Water Mass Flow
x	Axial coordinate
ρ_p	Droplet density

*Address all correspondence to this author (Email: schmid@td.mw.tum.de).

INTRODUCTION

Combustion instabilities are subject of several research projects at the *Lehrstuhl für Thermodynamik* at the *Technische Universität München*. In collaboration with *General Electric Global Research*, the acoustic properties of the exhaust system of a gas turbine single can combustion test rig have been investigated. Special focus is made on the influence of water injection into the test rig. Therefore, a test rig is build up representing a downscaled single can combustion test rig. Water can be injected via a special injection unit. A siren is used to excite the system at different frequencies. Dynamic pressure sensors measure pressure fluctuations to reconstruct the one dimensional wave field in the impedance tube upstream of the so-called transition cone. Reflection coefficients and acoustic fluxes are calculated at the inlet to the cone to determine the acoustic properties of the downstream system.
In the following, a brief introduction to some theoretical fundamentals, which are necessary for the understanding of this paper, is given. Then, the test rig is described in detail. Experimental results are shown in the last section. The different subsections present the results of the influence of air mass flow, water mass flow, cylinder size and bar element.

THEORETICAL FUNDAMENTALS

In the first section of this chapter, an introduction to one-dimensional acoustics in ducts is given. Then, the *Multi Microphone Method* is presented as well as the influence of two phase flow on the sonic velocity. At the end of this chapter, the network modeling approach is introduced shortly.

One Dimensional Acoustic Theory

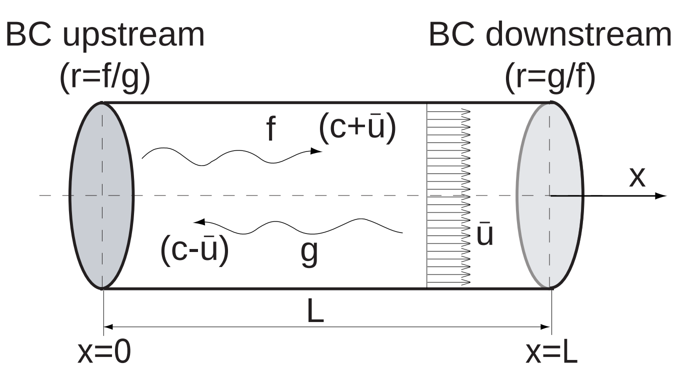

FIGURE 1: 1D WAVE PROGATION IN THE PRESENCE OF A MEAN AXIAL FLOW

The acoustic field of straight ducts is a superposition of the Riemann invariants f and g, which are the solutions of the wave equation. These may be interpreted as acoustic waves propagating in the downstream and upstream directions, respectively, as presented in Fig. 1. In terms of the Riemann invariants f and g, the complex acoustic pressure amplitude $\hat{p}$ is defined as

$$\frac{\hat{p}(x)}{\bar{\rho}c} = f \cdot e^{-ik_x^+ x} + g \cdot e^{-ik_x^- x} \tag{1}$$

and the corresponding complex acoustic velocity amplitude $\hat{u}$ as

$$\hat{u}(x) = fe^{-ik_x^+ x} - ge^{-ik_x^- x}. \tag{2}$$

In Eqn. 1, the term $\bar{\rho}c$ is the specific impedance of the considered medium. The parameters $k_x^\pm$ are the axial wave numbers, which describe the wave form of the acoustic mode in axial direction for pure longitudinal modes.

$$k_x^\pm = \pm\frac{\omega}{c \pm \bar{u}} = \pm\frac{\omega}{c\,(1 \pm M)} \tag{3}$$

As acoustic damping is neglected, the wave numbers are purely real without any imaginary part.
The reflection coefficient r in the downstream direction is defined in terms of the Riemann invariants as

$$r = \frac{g}{f}. \tag{4}$$

It describes the ratio of the acoustic wave propagating upstream (g) to the downstream traveling wave (f) as a complex value at a specific reference plane.
The acoustic flux I describes the amount of energy which passes the reference plane per unit time. In the case of a potential flow with $M = \frac{\bar{u}}{c}$, its time averaged value can be expressed by

$$\langle I \rangle = \frac{\bar{\rho}c}{2}\left(|f|^2 (1+M)^2 - |g|^2 (1-M)^2\right) \tag{5}$$

as it was shown in [1]. Here, the acoustic flux is a dimensional value. It can also be written in a non-dimensional form (Equ. 6), depending just on the Mach number M and the norm of the downstream reflection coefficient $|r|$.

$$\langle K \rangle = \frac{\langle I \rangle}{\langle f^2 \rangle}\frac{1}{\bar{\rho}c(M+1)} = 1 - |r|^2 \left(\frac{1-M}{1+M}\right)^2 \tag{6}$$

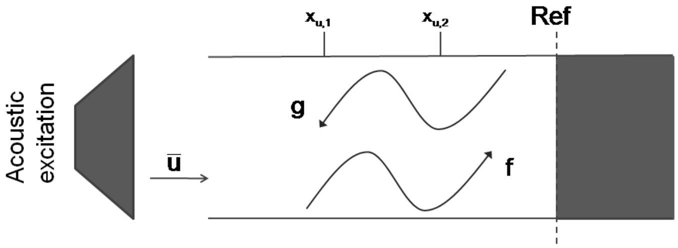

FIGURE 2: MULTI MICROPHONE METHOD WITH ONE EXCITATION SOURCE

Multi microphone method

The *Multi Microphone Method* (MMM) is a common method to determine wave fields in simple acoustic devices. In consequence, acoustic transfer matrices and reflection coefficients of acoustic systems can be calculated. It has been successfully used in previous projects of the *Lehrstuhl für Thermodynamik* of the *Technische Universität München*, as presented for example in [2] and [3]. Transfer matrices describe the change of pressure and velocity waves caused by specific devices, such as ducts, area expansions or flames. In the present context, the *Multi Microphone Method* has been used to reconstruct the wave field in the upstream duct of the test rig. Then, the reflection coefficient and the acoustic fluxes at the reference plane, the interface between upstream duct and the area change, are determined. Acoustic excitation of the test rig is realized through a siren (Fig. 2).

Dynamic pressure sensors, placed between the siren and the reference plane, detect the pressure fluctuations caused by the acoustic waves. By means of Equ. 1 and the independent pressure fluctuations of at least two sensors, the Riemann invariants can be calculated. To achieve higher accuracy, six sensors are used to measure the pressure fluctuations. With a non-linear *Levenberg-Marquardt Fit*, f and g are calculated and therefore, the complete wave field is reconstructed. Using f and g, the reflection coefficient r and the acoustic fluxes $\langle I \rangle$ and $\langle K \rangle$ are determined at the desired reference plane.

Sonic velocity in two phase flow

As the test rig operates under cold conditions (without combustion or preheating), evaporation of the injected water droplets can be neglected. Hence, a two phase flow of air and liquid water droplets exists in the downstream part of the test rig. Following the theory presented in [4], the sonic velocity strongly differs between single and two phase flow. The sonic velocity strongly decreases with even only a small volume fraction of water. It reaches a miminum and finally rises to the sonic velocity of pure water (Fig. 3). As derived in [4], the sonic velocity in a two phase

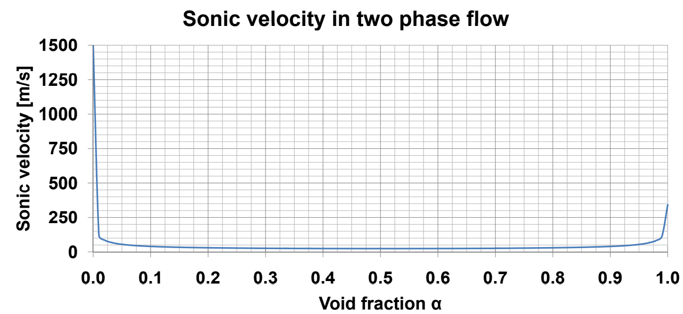

FIGURE 3: SONIC VELOCITY OVER VOID FRACTION FOR TWO PHASE FLOW OF AIR AND WATER

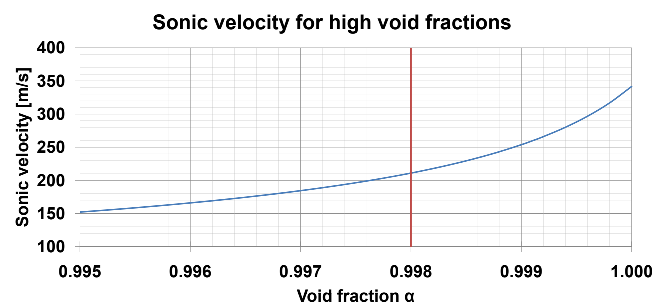

FIGURE 4: SONIC VELOCITY OVER VOID FRACTION FOR $\alpha = 0.995 - 1$

flow without heat and mass transfer can be calculated (Equ. 7).

$$\frac{1}{c^2} = (\rho_L \alpha_L + \rho_G \alpha_G) \left[\frac{\alpha_G}{\rho_G c_G^2} + \frac{\alpha_L}{\rho_L c_L^2} \right] \tag{7}$$

The void fractions

$$\alpha_G = \frac{V_G}{V_L + V_G} = 1 - \alpha_L \tag{8}$$

describe either the volumetric fraction of air compared to the total volume (α_G) or the volume of water compared to the total volume (α_L). $\alpha_G = 0$ corresponds to solely liquid water and $\alpha_G = 1$ is pure air. Henceforth, only the void fraction of gas α_G is considered, therefore α is equal to α_G. As shown in Fig. 3, the sonic velocity decreases rapidly with only a small void fraction of water. The highest mass fraction achieved in this project is about $3 \frac{kg_{water}}{kg_{air}}$, which corresponds to $\alpha = 0.993$. Even though the void fraction of the mixture in the test rig is just below 1, Fig. 4 shows that the change of sonic velocity is quite remarkable within the limits of this theory. The vertical red line in Fig. 4 indicates the

void fraction of the case with $AMF = 400\frac{g}{s}$ and $WMF = 300\frac{g}{s}$ which corresponds to $\alpha = 0.998$. As the reflection coefficient depends on the sonic velocity, it can be expected that the reflection coefficient changes with the amount of water injected in the system.
The limits of this theory got very clear during the analysis of the experimental results. As already mentioned, the presented equation for the sonic velocity and the according graphs are valid for highly dispersed water, like fog, where the droplets follow the acoustic velocity fluctuations without slip. This implies that the diameter of the injected water droplets has to be quite small. To quantify the influence of the droplet diameter, the Stokes number will be used in this report. More detailed models for the sonic velocity of two phase flows can be found in [4].

Network Model

The network model is used to better understand the influence of two phase flow on the acoustic properties of the test rig. In this paper, only a short description is given. More detailed information on this approach can be found in [5] and [6]. Acoustic systems, like ducts and area expansions, can be described via acoustic transfer matrices, which couple acoustic fluctuations at the inlet of the system to the corresponding values at the outlet. Adding up several transfer matrices, even very complex systems as complex combustion test rigs can be modeled.
In a numerical part of the project, the different parts of the test rig described in the next section are modeled and free parameters are adapted to finally well reproduce the experimental results. Then, the above presented equation for the sonic velocity (Equ. 7) is used to theoretically study the influence of different acoustic properties in the downstream system. The sonic velocity changes the real part of the wave number and therefore has the same influence as a different length of the system. The consequence in both cases are different propagation times for the waves from the area expansion to the outlet and back. This results in a frequency shift of the minima of the reflection coefficient.
Additionally, the influence of a higher damping is studied. Therefore, the imaginary part of the wave number is artificially increased. These results are used to explain the behavior of the experimental results.

TEST RIG SETUP

Overview

The test rig consists of a duct, an area expansion with the water injection system followed by a cone, to reduce the cross section to the same diameter of the upstream pipe, and a ball valve at the end of a second duct. A siren is used to excite the flow in the test rig. In a second test case, a bar element is mounted between the upstream pipe and the area expansion to impose choked flow conditions as in the original gas turbine, where the turbine inlet is choked. The reference plane for the calculation of the reflection coefficients and acoustic fluxes is just upstream of the cylinder, which is indicated by the dashed red line in Fig. 5. Both test cases, with and without the bar element, are presented in this figure. The different parts, except the ball valve, are shown in Fig. 6. Table 1 summarizes the geometrical dimensions of the test rig.

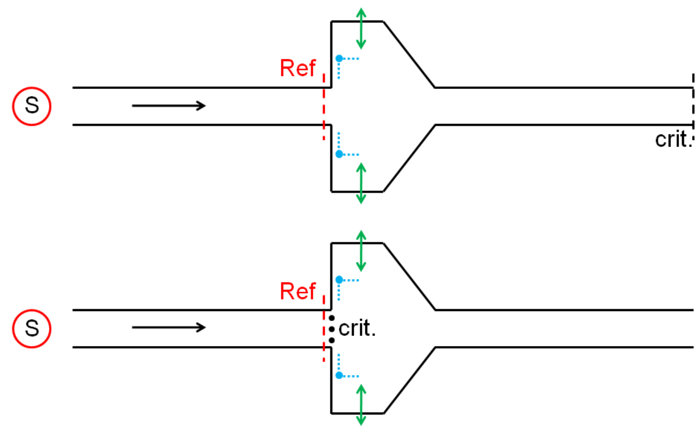

FIGURE 5: SKETCH OF THE TEST RIG WITHOUT (TOP) AND WITH (BOTTOM) BARS

	diameter $[mm]$	length $[mm]$
upstream pipe	64	1191
downstream pipe	64	1020
big cylinder	190	73
small cylinder	140	73
big cone	190	110
small cone	140	110

TABLE 1: GEOMETRICAL DIMENSIONS OF THE TEST RIG

Siren excitation

A siren is used to excite the flow in the test rig at specific frequencies to study the reflection coefficient and the acoustic fluxes. The frequency range is chosen from 150Hz up to 700Hz. At higher frequencies, the cut-on frequency of the first tangential mode is reached. Consequently, higher modes have to be taken into account for the reconstruction of the wave field. Therefore, the assumption of one dimensional acoustics in the test rig would not be valid any more.

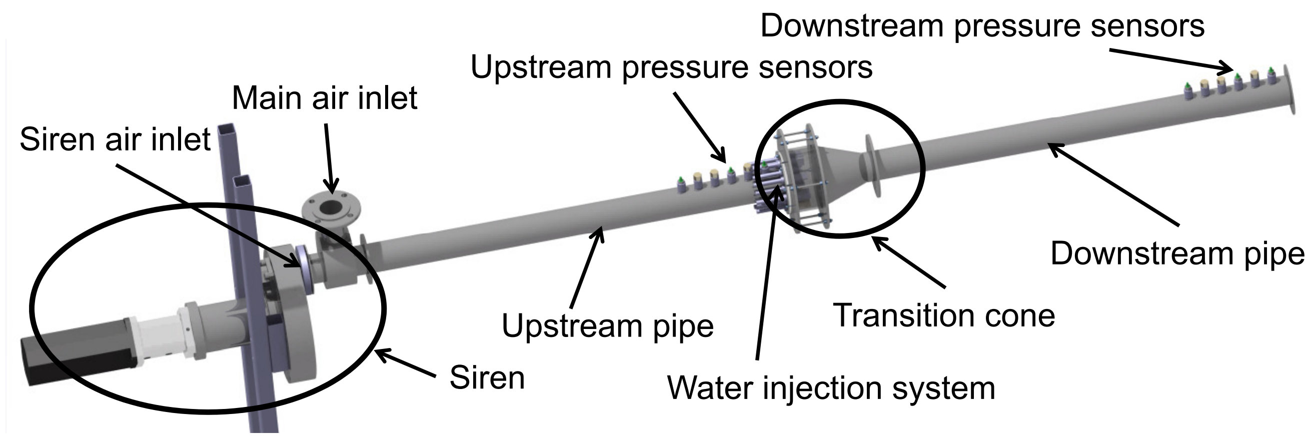

FIGURE 6: TEST RIG WITH THE DIFFERENT PARTS

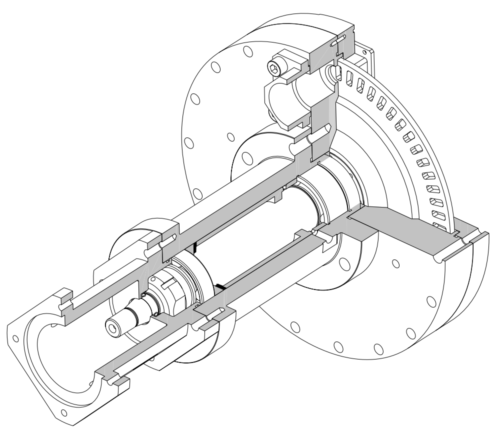

FIGURE 7: SECTIONAL VIEW OF THE SIREN

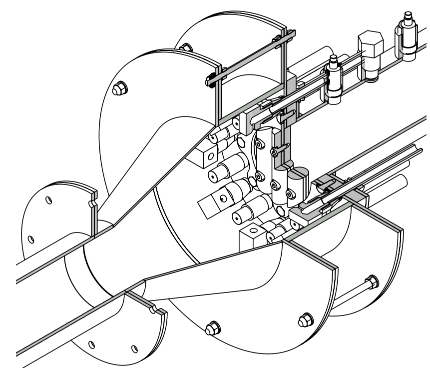

FIGURE 8: SECTIONAL VIEW OF THE SMALL CYLINDER WITH BAR ELEMENT

The siren consists of a motor which is directly coupled to a siren disk with 56 holes and an outer diameter of $260mm$. Consequently, the revolution speed of the motor determines the excitation frequency. A sectional view of the siren is given in Fig. 7.

Upstream and downstream duct, transition cone and ball valve

The main part of the test rig consists of two ducts, which are installed upstream and downstream of a so-called transition cone. The upstream and downstream pipes have similar diameters and six connections to insert probes.

Two different diameters for the cone are used with area ratios of $A_{small\ cylinder}/A_{duct} = 4.7$ and $A_{big\ cylinder}/A_{duct} = 8.8$. The length of the cylinder and the cone are chosen in relation to the diameter of the upstream pipe to achieve geometrical similarity. For a visible control of the water injection, the cylinder is made of acrylic glass. The flange connecting the upstream pipe to the cylinder also includes the connections for the nozzles of the water injection system. They reach down to approximately the middle of the cylinder. The first set of nozzles (type: Lechler Full Cone Nozzle 460.404) injects in the axial, the other in radial direction (type: Lechler Full Cone Nozzle 422.406) to the flow. Eight nozzles of both types are evenly distributed in a circle around the pipe outlet. The outlet of the radial spraying nozzles faces inwards carrying away the injected water by the air mass flow immediately. A metallic cone is used to ensure a smooth transition from the cylinder to the downstream pipe. Figure 8 gives a sectional view of the transition cone with the bar element and the small cylinder as well as the water injection nozzles.

A ball valve is attached to the end of the test rig. The port diameter is adjusted manually with a lever to ensure a pressure of $p = 2bar$ in the test rig resulting in a choked flow at the outlet. For the test case with the bar element, the valve is fully open, so that ambient pressure is present in the downstream duct.

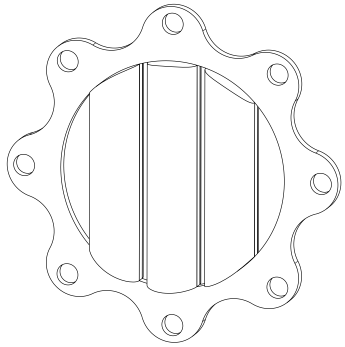

FIGURE 9: BAR ELEMENT

Bar element

The second test case includes a bar element (Fig. 9) at the reference plane to generate equal flow conditions in the test rig compared to real gas turbines, as the first stage of the turbine is choked. Consequently, the cross-section of the bar element is calculated to have $M = 1$ in the test case with an air mass flow of $\dot{m}_{air} = 400\frac{g}{s}$ at an upstream pressure of about $2bar$.

EXPERIMENTAL RESULTS

A total of 37 measurements are performed for the investigation of the influence of air and water mass flow, cylinder size and bars on the reflection coefficient and the acoustic flux. The reflection coefficient r, the dimensional $\langle I \rangle$ and non-dimensional $\langle K \rangle$ acoustic flux are plotted as functions of the excitation frequency. For better comparability of the results, reflection coefficient, dimensional and non-dimensional acoustic flux are plotted in one diagram for each set of measurements. The bar element is only used in the section "Influence of Bar Element". All other test cases are performed without bar element. In the diagrams, where the droplet diameters are indicated, the estimated values for the axial (AN) and radial (RN) nozzles are presented.
First, one experiment is repeated 5 times to investigate the reproducibility of the measurements. Relative deviations less than 0.5% are found. These very small deviations are due to the high number of used pressure transducers (6) compared to the theoretically needed number (2). It can be concluded that the results are reproduced very well.

Influence of Air Mass Flow

Investigations on the influence of different air mass flows on the system are carried out with and without injected water. Table 2 gives an overview of the Mach numbers in the upstream pipe for the different air mass flows. An air mass flow of $AMF = 50\frac{g}{s}$ is present in the test cases 19 and 20. With a static pressure of $p = 2bar$ in the upstream duct, the Mach number is very low ($M_{19} = 0.02$). In all other test cases, much higher Mach numbers

Air mass flow $\left[\frac{g}{s}\right]$	Mach number
50	0.02
300	0.11
400	0.15
500	0.19

TABLE 2: MACH NUMBERS IN UPSTREAM PIPE IN SUBJECT TO THE AIR MASS FLOW

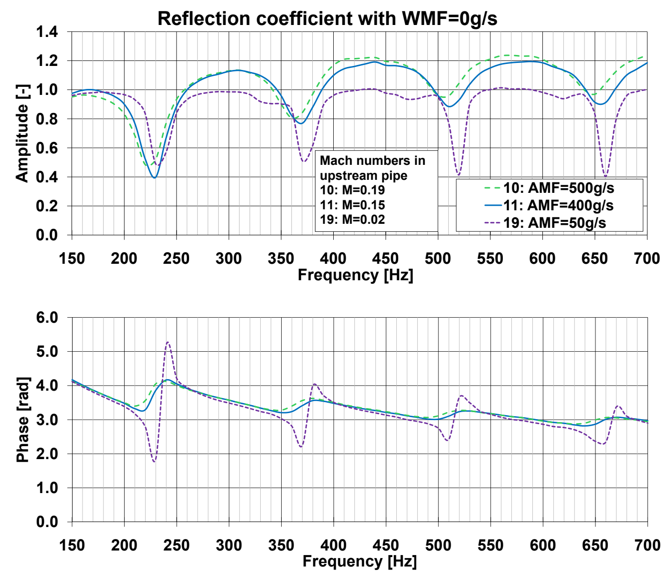

FIGURE 10: INFLUENCE OF AMF ON REFLECTION COEFFICIENT. ALL TESTS HAVE $WMF = 0\frac{g}{s}$ AND THE SMALL CYLINDER.

like $M_{10} = 0.19$ and $M_{11} = 0.15$ appear due to higher air mass flows.
Each of the Figs. 10 and 11 shows 3 separate curves, which have different air mass flows but the same water mass flow. Figure 10 shows different air mass flows without any injected water and Fig. 11 a variation of air mass flow with a water mass flow of $WMF = 150\frac{g}{s}$. Both diagrams show curves with a similar behavior. Experiments with higher air mass flow have higher amplitudes but smoother curves. "Smoother" means in this context that the difference between local minima and maxima decreases. This can be verified by the phase which shows lower peaks with increasing air mass flow. It is observable that the amplitude of the reflection factor of test cases 19 and 20, with very small Mach number, never exceed 1. A frequency shift of the minima not exceeding $20Hz$ in relation to curve 20 is distinguishable in the

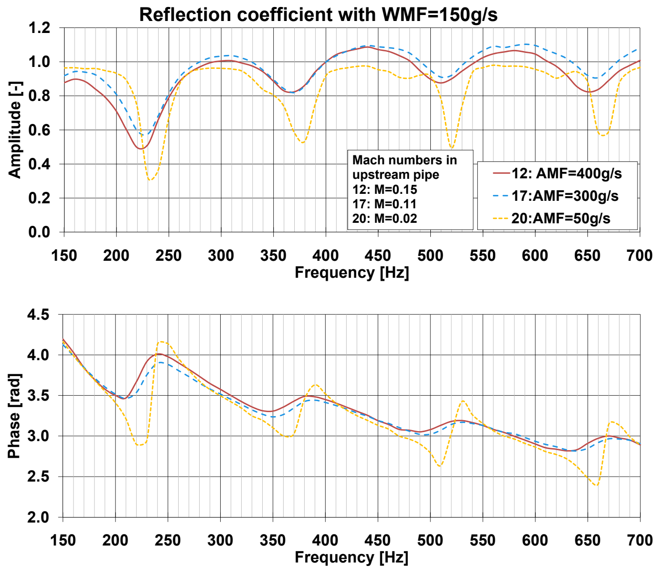

FIGURE 11: INFLUENCE OF AMF ON REFLECTION COEFFICIENT. ALL TESTS HAVE $WMF = 150\frac{g}{s}$ AND THE SMALL CYLINDER.

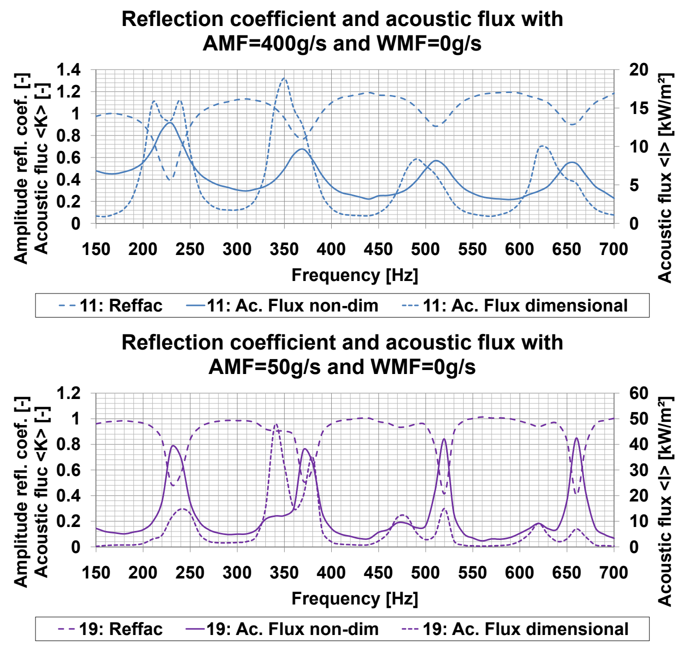

FIGURE 12: INFLUENCE OF AMF ON ACOUSTIC FLUX. ALL TESTS HAVE $WMF = 0\frac{g}{s}$ AND THE SMALL CYLINDER.

amplitude and phase diagrams.

With higher air mass flow in the pipe the velocity of the air increases and therewith also the Mach number. The increase of curves 10, 11, 12 and 17 above a reflection coefficient of $r = 1$ is a phenomenon caused by convection, more precisely by different wave propagation velocities. The downstream traveling wave (f) propagates with a velocity of $c+\bar{u} = c(1+M)$, whereas the upstream traveling (g) has a velocity of $c-\bar{u} = c(1-M)$. The difference of the wave propagation velocities in the cases 19 and 20 is much lower due to the small Mach number. The minima indicate the eigenfrequencies of the downstream system. In the test cases 19 and 20, the velocity is much smaller than in the other cases. Friction losses correlate with the velocity of the fluid. Therefore, they are more important in test cases with higher air mass flows. This leads to higher damping of the flow, which results in smoother curves.

These conclusions could be drawn by varying the length of the downstream system and the loss coefficients in the network model. The model clearly indicates that the periodic behavior with local minima and maxima is due to the reflection at the downstream end. Increasing the Mach number without considering losses only leads to higher local maxima. Adding a pressure loss at the area expansion leads to an upward shift of the local minima and a downward shift of the maxima, which is referred to in the following as "smoother curve".

Figure 12 combines the reflection coefficient and acoustic flux of measurements with no water, small cylinder and different air mass flows. Especially in the curve of the dimensional acoustic flux of measurement 19, double peaks are visible. The second maximum of these double peaks occur approximately at the same frequency as the minima of the reflection coefficients does. The maxima of the non-dimensional acoustic flux are located at the same frequencies, so the energy transport through the reference plane is influenced by the reflection coefficient. The less energy is reflected in the reference plane (which is a minimum in the amplitude of the reflection coefficient), the more energy propagates downstream. The other peaks of the dimensional acoustic flux, which do not correlate with the reflection coefficient, are located at the eigenfrequencies of the whole test rig. At these frequencies, the system absorbs much more energy, so the pressure amplitudes and consequently the acoustic flux is higher. For curve 11 both phenomena occur at frequencies which are close to each other, so in the graph they coincide to one expanded peak.

Influence of Water Mass Flow

The following figures show the influence of different water mass flows on the reflection coefficient and the acoustic flux. Each of these diagrams includes several curves of measurements with the same air mass flow but varying water mass flows. The volume flow rate of water has an influence on the droplet diameter. According to the theory of sonic velocity in two phase flows, the injected water reduces the sonic velocity of the mixture if the droplets are of considerable small size. Table 3 gives the void

AMF $[\frac{g}{s}]$	WMF $[\frac{g}{s}]$	α	μ
50	150	0.9927	0.75
400	50	0.9997	0.11
400	300	0.9982	0.43

TABLE 3: VOID AND MASS FRACTION FOR STANDARD CASES.

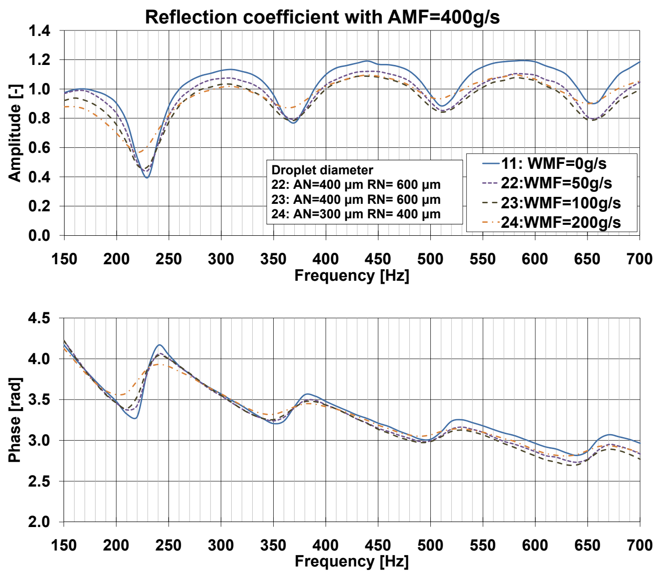

FIGURE 13: INFLUENCE OF WMF ON REFLECTION COEFFICIENT. ALL TESTS HAVE $AMF = 400\frac{g}{s}$ AND THE SMALL CYLINDER.

and mass fractions for the different mass flow rates. In Fig. 13, the four curves have an air mass flow of $AMF = 400\frac{g}{s}$ but different water mass flows of $WMF = 0\frac{g}{s}$, $50\frac{g}{s}$, $100\frac{g}{s}$ and $200\frac{g}{s}$. Both figures, amplitude and phase, show that flows with higher water mass flow rate have smoother curves which means that they are more damped. This is due to the friction losses caused by the different velocities of air and injected water. The more water is injected into the air flow, the more contact surface between water and air is available. Figure 14 shows reflection coefficients of measurements with the same conditions as in Fig. 13, except different water mass flows of $WMF = 0\frac{g}{s}$, $150\frac{g}{s}$ and $300\frac{g}{s}$. The amplitude diagram shows a damping of measurements 12 and 13 (both with injected water) compared to the case 11 (without injected water). This damping is indicated by the lower maximum and higher minimum which results in a smoother curve in the amplitude- as well as in the phase-diagram. The phase diagram of curve 13 with the most water mass flow is much smoother

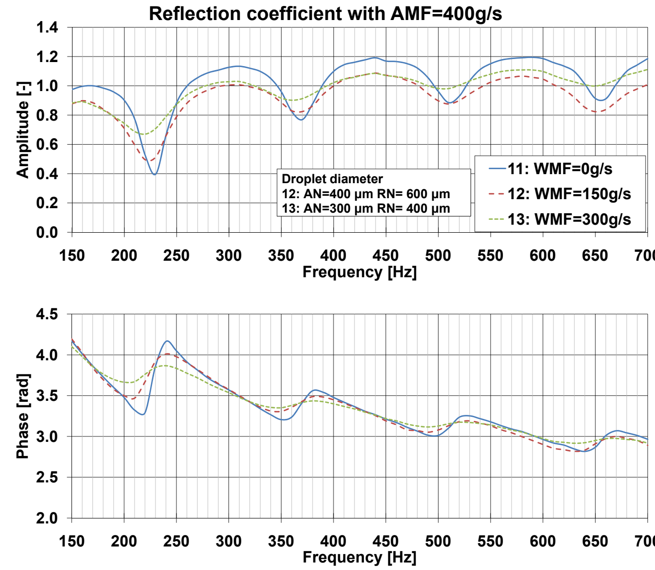

FIGURE 14: INFLUENCE OF WMF ON REFLECTION COEFFICIENT. ALL TESTS HAVE $AMF = 400\frac{g}{s}$ AND THE SMALL CYLINDER.

than 12, which indicates that the water mass flow causes damping. However, the maximum of 13 in the amplitude diagrams is generally higher than 12, what on the contrary suggests a lower damping. A slight shift of the minima to the left of about $10Hz$ to $20Hz$ of curves 12 and 13 compared to 11 is detectable in the diagrams.

As explained before, the injection of water into air can decrease the sonic velocity. From a numerical study using the network modeling approach and applying the previously presented sonic velocity for a two phase flow for the downstream system, it was shown that the shift is much greater than the $20Hz$ detectable in the diagrams. It results from a different wave number in the downstream system and has therefore the same effect as a different length of this system. An explanation, why this does not occur in the experiments, can be given using the Stokes number. The theory of the change of sonic velocity is just valid for a homogeneous mixture. This means that the droplets must be so small that they behave like particles of the air. This is valid for a Stokes number of $St \leq 1$. It can be expressed as a relation between the droplet relaxation time and the acoustic frequency.

$$St = \frac{\rho_p d_p^2 f}{18\eta k} \tag{9}$$

For $St = 1$, the droplet diameter can be calculated to $d_{100Hz} = 28\mu m$ at a frequency of $f = 100Hz$ and to $d_{700Hz} = 11\mu m$ at a frequency of $f = 700Hz$. The diameter of the droplets was not

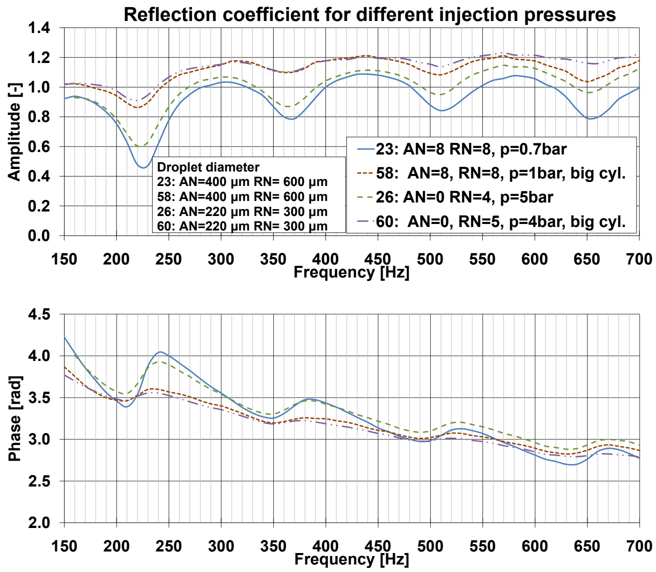

FIGURE 15: INFLUENCE OF THE WATER INJECTION PRESSURE ON REFLECTION COEFFICIENT: ALL TESTS HAVE $AMF = 400\frac{g}{s}$, $WMF = 100\frac{g}{s}$ AND THE SMALL OR BIG CYLINDER.

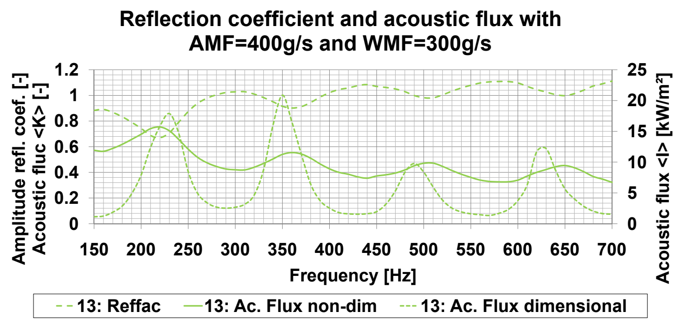

FIGURE 16: INFLUENCE OF WMF ON ACOUSTIC FLUX. THE TEST HAS $AMF = 400\frac{g}{s}$ AND THE SMALL CYLINDER.

measured, especially not in the case with a surrounding air flow as it is the case in the present test rig. Consequently, no detailed values for the diameters can be given. According to measured diagrams from the manufacturer, the droplet diameters for the corresponding injection conditions (mass flow rate and pressure drop) can be estimated being about $d = 200\mu m$ for the used nozzles, which is much higher than the previously calculated diameters. The Stokes number for the achievable droplet diameters by these nozzles are $St_{100Hz} \approx 80$ and $St_{700Hz} \approx 5600$. It can be concluded that the droplets cannot follow the acoustic fluctuations of the surrounding air. This means that the acoustic waves just propagate through the air with the sonic velocity of the air. Measuring the droplet diameter distribution would increase the accuracy of interpretation in future projects.

The water still has a damping effect due to friction losses, as described before. This damping can be seen in the phase graph, where measurement 13 has the smoothest shape. However, in the amplitude diagram, curve 13 is generally higher than curve 12, which means that the reflection coefficient has a higher amplitude.

In the usual test configuration, water mass flow is adjusted by a valve just upstream of the mass flow meter. However, this valve reduces the pressure considerably so that the gauge pressure between water upstream of the nozzles and air in the pipe is very small, as it can be seen in Fig. 15 for measurements 23 and 58. As explained before, the droplet size depends on the injection pressure of water. To have a higher injection pressure but a constant water mass flow of $WMF = 100\frac{g}{s}$, the valve upstream of the flow meter is kept wide open and some nozzles are shut completely by their own valve. This made it possible to take the measurements 26 and 60, shown in Fig. 15. The measurements for the big cylinder, 58 and 60, and for the small cylinder configuration, 23 and 26, have to be compared. In both cases, they have an identical air and water mass flow. If the influence of droplet size is negligible, the curves should be on top of each other. However, this figure illustrates clearly that, with a higher injection pressure, the reflection coefficient has a higher amplitude. It can be concluded that the smaller the droplets are, the higher are the amplitudes and the smoother is the phase of the reflection coefficients.

Transferring this conclusion to Fig. 14, the behavior of measurement 13 can be explained. The water mass flow of $WMF = 300\frac{g}{s}$ is the maximum possible, so the water control valve is fully open and no pressure drop occurs. The injection pressure is much higher than during the other measurements. Besides the higher water mass flow, yielding smoother curves, the droplet size is much smaller, resulting in an upward shift. In the graph of the phase, the influence of droplet size is not detectable, as the droplet size and the amount of water have the same effect on the phase. The reflection coefficient, the dimensional and non-dimensional flux of measurement 13 are plotted in Fig. 16. This figure has to be compared with measurement 11 in Fig. 12. The acoustic flux confirms that a higher water mass flow has a damping effect on the flow. The more water is in the system, the smoother is the shape of the non-dimensional acoustic flux. The high peaks of the acoustic flux are induced by the eigenfrequencies of the system. This influence seems to be more pronounced the more water is in the system. The peaks of curve 13 are higher than the ones of curve 11 and the shift to the left is more distinctive.

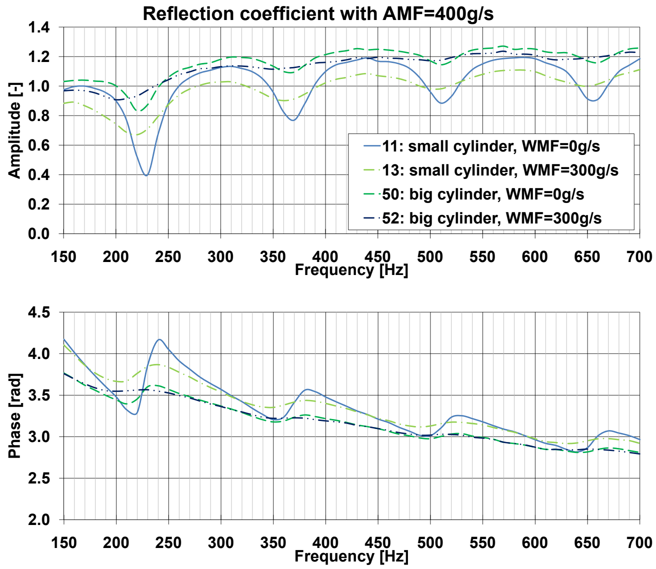

FIGURE 17: INFLUENCE OF THE CYLINDER SIZE ON REFLECTION COEFFICIENT. ALL TESTS HAVE $AMF = 400\frac{g}{s}$ AND $WMF = 0\frac{g}{s}$ OR $WMF = 300\frac{g}{s}$.

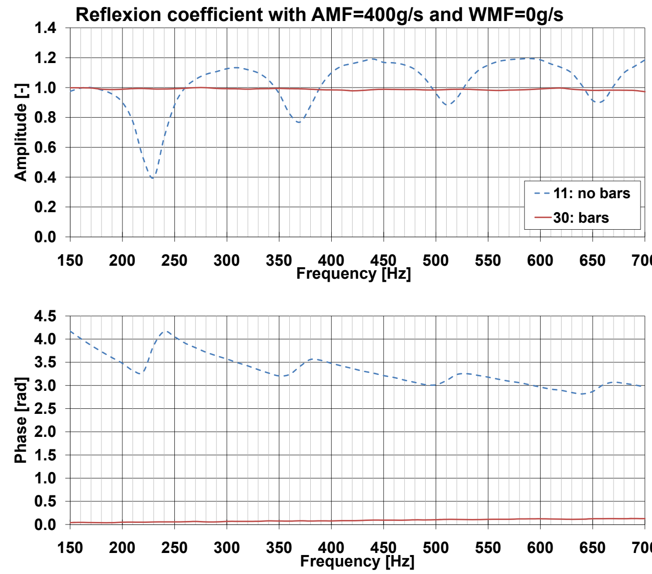

FIGURE 18: INFLUENCE OF A BAR ELEMENT ON REFLECTION COEFFICIENT. ALL TESTS HAVE $AMF = 400\frac{g}{s}$, $WMF = 0\frac{g}{s}$ AND THE SMALL CYLINDER.

Influence of Cylinder Size

As indicated before, the size of the cylinder seems to have an impact on the flow and therefore on the reflection coefficient and acoustic flux. Figure 17 shows four different measurements which help to figure out the influence of the size of the cylinder element. The small cylinder element is used for measurements 11 and 13 whereas measurements 50 and 52 have the big cylinder. For each cylinder size, measurements without water and with $WMF = 300\frac{g}{s}$ are analyzed. Comparing the small and big cylinder, with the corresponding water mass flow, it can be observed that the reflection coefficient has a higher but smoother amplitude for the bigger cylinder. The phase curve of the bigger cylinder is shifted downwards compared to the curve of the smaller cylinder. No displacement of the minima is found.

In general the bigger cylinder has a higher damping effect. One explanation for this phenomena is that the area expansion from the pipe to the cylinder is bigger. As flow losses are proportional to this ratio, the bigger cylinder yields higher damping. Additionally, the upward shift is due to the higher area ratio of the bigger cylinder. This can be shown analytically and with the network model.

Influence of Bar Element

The installation of bars in the test rig imposes sonic flow conditions at the reference plane ($M = 1$). Therefore, the mean flow velocity is equal to the sonic velocity and no acoustic information can propagate upstream through the bars. Figure 18 shows the results of the second test case with the same air and water mass flow but with and without bars. The reflection coefficient of the test rig with the small cylinder element, an air mass flow of $AMF = 400\frac{g}{s}$ and no water mass flow is displayed. The amplitude is almost constantly at 1 and the phase at 0. No strong amplitude variations are visible as in the curves of the reflection coefficients without bars.

As already mentioned at the beginning of this section, no information from the downstream flow can get through the choked area of the bars and influence the upstream flow. This is affirmed by the results, where all reflection coefficients are the same regardless of whether water is injected or which air mass flow or cylinder is used. Marble and Candel [7] predict that the reflection coefficient for choked compact nozzles is $r = 1$. The bars in the test rig act like a nozzle and the measurements give roughly an amplitude of $|r| = 1$ and a phase of $\angle r = 0$ as expected before. For measurement 30, the bars are installed and the flow is choked. The non-dimensional acoustic flux of the measurements with bars is just a straight line as plotted in Fig. 19 . This is due to the fact that this acoustic flux only depends on the reflection coefficient. The progress of the curve of dimensional acoustic flux is quite different, as curve 30 shows high peaks. The location of the peaks are at different frequencies than the peaks of measurement 11. In measurement 11, the energy transport through the reference plane due to reflection and eigenfrequencies is shown, as explained in the sections before. The peaks of curve 30 indicate the eigenfrequencies of the system with bars. As no information can propagate upstream through the choked area, these eigenfrequencies are solely the ones of the upstream

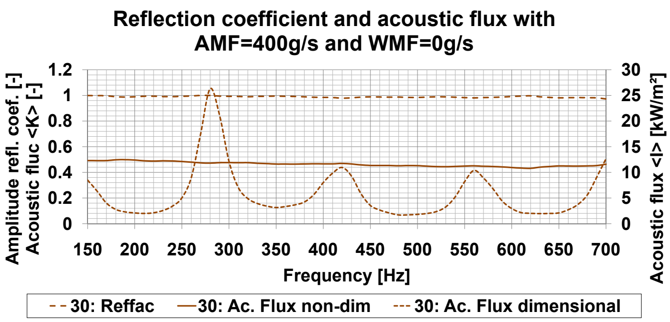

FIGURE 19: INFLUENCE OF A BAR ELEMENT ON ACOUSTIC FLUX. THE TEST HAS $AMF = 400\frac{g}{s}$, $WMF = 0\frac{g}{s}$ AND THE SMALL CYLINDER.

part of the system.

CONCLUSION

The results of an experimental study on the acoustic properties of the exhaust system of a single can combustion test rig have been presented in this paper. Especially, the influences of water injection have been addressed. After the introduction of some theoretical fundamentals, the design of the test rig representing a downscaled single can combustion test rig was outlined. The results of the study showed very clearly that the sonic velocity does not change due to the water injection, which was expected before. This is due to the fact that the droplets in the test rig are too big to follow the acoustic fluctuations of the surrounding air. This can be shown by comparison to numerical results obtained with the network model. The main difference in acoustic properties results from an increased damping of the two phase flow, which also depends on the droplet diameter. Increasing the mass flow and therefore increasing the Mach number in the test rig results in higher reflection coefficients, which can even exceed one. The influence of the cylinder of the transition cone has been also shown as well as the influence of a bar element. A bigger diameter of the cylinder also results in higher damping due to the higher pressure loss in the area expansion between upstream pipe and transition cone. The choked flow through the bar element modeling the choked inlet of the turbine, behaves as expected. No influence of cylinder size or water injection can be seen with the bar element as no information can propagate upstream through the choked plane.

A more detailed study on the influence of the droplet diameter on the acoustic damping is necessary to quantify the dependency of damping and sonic velocity more precisely. Finally, it should be possible to numerically predict the influence of water injection on the acoustic behavior of a single can test rig. All other influences can already be modeled satisfactorily with a network approach.

ACKNOWLEDGMENT

Thanks go to *General Electric Global Research* for the financial support of this project.

REFERENCES

[1] Pieringer, J. E., 2008. *Simulation selbsterregter Verbrennungsschwingungen in Raketenschubkammern im Zeitbereich, PhD Thesis, TU München*.

[2] Neunert, U., 2009. *Thermoakustische Stabilität einer Reisemobilheizung, PhD Thesis, TU München*.

[3] Fischer, A., 2003. *Hybride, thermoakustische Charakterisierung von Drallbrennern, PhD Thesis, TU München*.

[4] Brennen, C. E., 2005. *Fundamentals of Multiphase Flow*. Cambridge University Press.

[5] Keller, J. J., 1995. “Thermoacoustic oscillations in combustion chambers of gas turbines”. *AIAA Journal*, ***volume 33, number 12***, pp. 2280–2287.

[6] Kopitz, J., Huber, A., Sattelmayer, T., and Polifke, W., 2005. “Thermoacoustic stability analysis of an annular combustion chamber with acoustic low order modeling and validation against experiment”. In Int’l Gas Turbine and Aeroengine Congress & Exposition, no. ASME **GT2005-68797** .

[7] Marble, F. E., and Candel, S. M., 1977. “Acoustic disturbance from gas non-uniformities convected through a nozzle”. *Journal of Sound and Vibration*, ***55***, pp. 225–243.